

Human Motion Driven Self-Powered Photodynamic System for Long-Term Autonomous Cancer Therapy

Zhuo Liu,[#] Lingling Xu,[#] Qiang Zheng,[#] Yong Kang, Bojing Shi, Dongjie Jiang, Hu Li, Xuecheng Qu, Yubo Fan,^{*} Zhong Lin Wang,^{*} and Zhou Li^{*}



Cite This: <https://dx.doi.org/10.1021/acsnano.0c00675>



Read Online

ACCESS |



Metrics & More



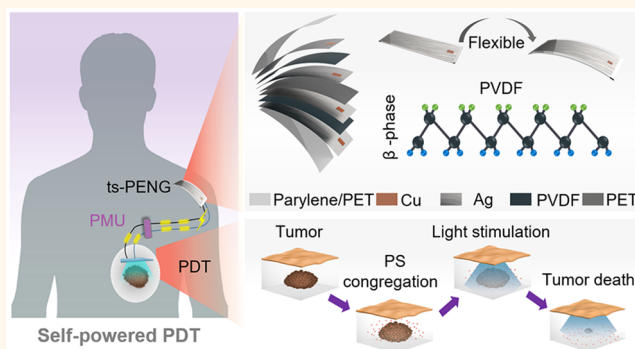
Article Recommendations



Supporting Information

ABSTRACT: Long-term and low-dose photodynamic therapy for treating tumors requires a sustainable energy supply. The power source technology of batteries and wireless charging for driving a light-emitting diode (LED) may cause inconveniences during treatment. In addition, the development of telemedicine and Internet medicine put forward higher demands on treatment methods, such as better patient compliance and autonomous management. Here, we show a self-powered photodynamic therapy (s-PDT) system with two different irradiation modes that can be autonomously managed by patients. The as-fabricated s-PDT system based on a twinning structured piezoelectric nanogenerator is powered by energy harvested from body motion and realizes effective tumor tissue killing and inhibition. As demonstrated at the cellular level, the s-PDT system can significantly suppress tumor cell growth with the pulsed light stimulation mode. When the miniature LED was implanted subcutaneously in mice with transplanted tumors, the s-PDT system led to significant antitumor effects by irradiation with intermittent continuous light stimulation mode for 12 days, and an 87.46% tumor inhibition rate was obtained. This innovative s-PDT system combined with two treatment modes may provide a great opportunity to develop wearable/implantable and self-controllable devices for long-term photodynamic therapy, which would be a promising method for clinical cancer treatment.

KEYWORDS: human motion, self-powered device, photodynamic therapy, cancer therapy, wearable



Cancer has a high mortality rate worldwide, and its treatment and recovery are a long-term process accompanied by a variety of medical skills.^{1–3} Currently, the light-based method for treating early cancers and residual tumors—photodynamic therapy (PDT)—is applied in the clinic with advantages of hypotoxicity, small wounds, and good selectivity,^{4–8} which includes photosensitizer (PS) and light of specific wavelengths.^{9–13} The mechanisms of killing tumor cells by PDT can be summarized into three aspects: generating reactive oxygen species (ROS), damaging the tumor-associated vasculature, and activating a defensive immune response.^{4,14,15} In an actual clinical treatment process, optical fibers are usually implanted adjoining the tumor location for short-term therapy with strong light exposure. Unfortunately, this high light intensity during the process of PDT may induce thermal damage for surrounding normal tissues, especially the nerves and blood vessels, which may cause unexpected organ dysfunction. However, with too little electroluminescence, the tumor

inhibition is rather insufficient.^{16–18} Therefore, how to balance irradiation-dose-based damage and the killing efficiency of tumor cells is always crucial for PDT.

To avoid the side effects due to excessive exposure of PDT and improve its safety and reliability, many efforts have been made for developing a PDT device with low irradiation dose.^{19,20} Recently, the metronomic PDT with weak light intensity was proposed by some research groups,^{21,22} which can avoid the high intensity illumination effect on organs and can improve the safety and reliability of PDT. This technology usually with the miniaturization of the system involves two

Received: January 23, 2020

Accepted: June 17, 2020

Published: June 17, 2020

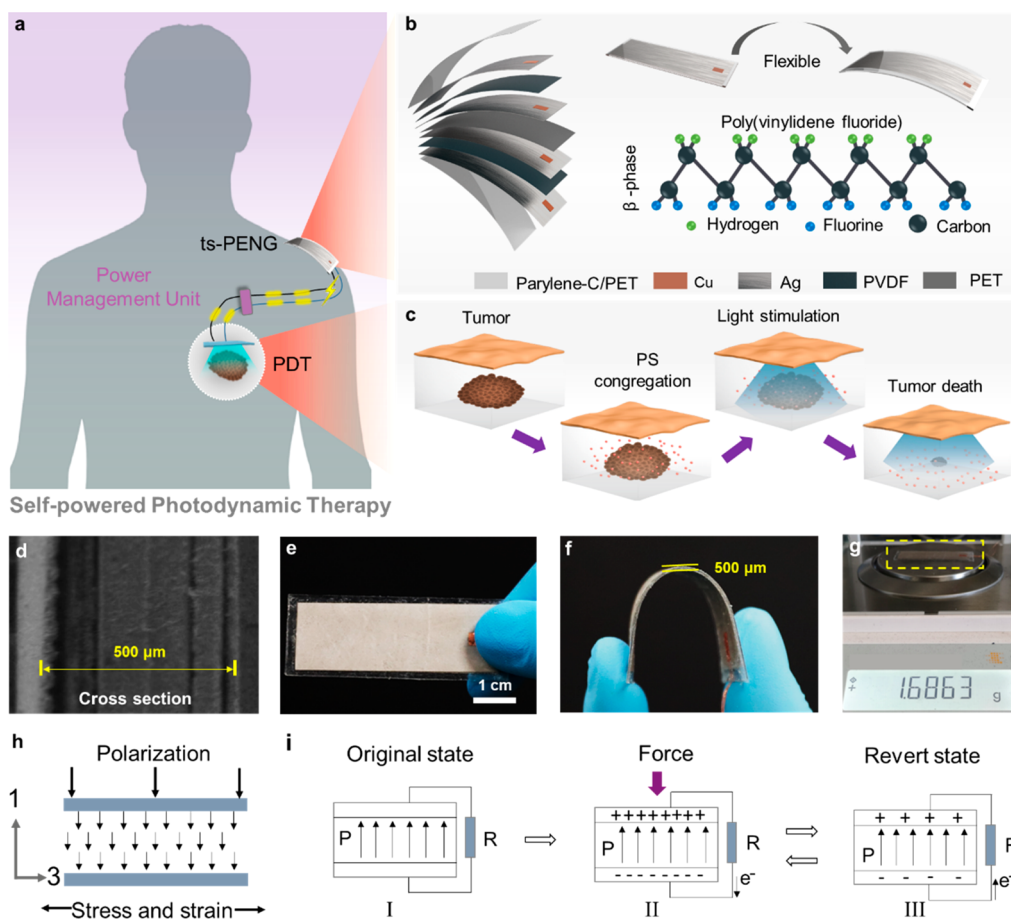


Figure 1. Overview of the s-PDT system. (a) s-PDT system consisted of ts-PENG, PMU, m-LED, and a photosensitizer. (b) 3D structure of the ts-PENG including encapsulation layers, PVDF, and substrate layers. (c) Apoptotic process of subcutaneous tumor tissue. (d) Cross-sectional SEM image of the ts-PENG. (e) Photograph of the ts-PENG in the original state. (f) Photograph of the ts-PENG in the bending state. (g) Weight display of the ts-PENG. (h) Schematic diagram of d_{31} working mode of the PVDF. (i) Working principle of the PVDF layer.

basic components, light-emitting diodes (LEDs) illuminant and a wireless power supply.²³ However, the wireless power supply for driving LED needs an energy transfer device with a specific working range, which will introduce time and space restrictions for patients. Therefore, considering the long-term photodynamic therapy process, it is not convenient for treatment in real-time and will lead to poor patient compliance. In addition, wireless coils receiving energy *in vivo* may also induce thermal effects on normal tissue surrounding the implantation site, which introduced additional potential risk factors in the process of the treatment. For these reasons mentioned above, a wearable or implantable PDT device with a sustainable power supply is urgently needed.

The booming technology of nanogenerators (triboelectric nanogenerators²⁴ and piezoelectric nanogenerators²⁵) has provided us with an effective approach to convert decentralized random mechanical energy into electric energy and has been utilized for sustainable power supply^{26–31} or active sensing.^{32–36} Recently, implantable and wearable nanogenerators have been developed and successfully harvested abundant biomechanical energy in the human body, such as joint motion,^{37–39} respiration,^{40–42} peristole,⁴³ blood flow, and heartbeat.^{44–46} Therefore, there is a great chance to convert these biomechanical energies into electricity for powering a PDT system and produce a promising way to overcome the

problems of poor compliance and restricted power supply of traditional long-term PDT methods.

Here, we demonstrate a self-powered PDT system (s-PDT system) for cancer treatment based on the wearable twinning structure piezoelectric nanogenerator (ts-PENG) encapsulated by Parylene-C, which has improved output performance. Compared with other energy sources such as a microbattery and wireless charging, the ts-PENG also has the following advantages, especially for patients who need long-term treatment. First, the ts-PENG has the advantages of simple structure flexibility and light weight, which are desirable characteristics for wearable medical devices. Second, the ts-PENG has good stability and long service life. It can supply power for a long time without periodic replacement, which is more convenient for patients and with better compliance. Third, the ts-PENG has favorable biosecurity. As an energy-harvesting unit, the ts-PENG can convert biomechanical energy from joint motion into electricity as a power source for driving the PDT system. Through a well-designed power management unit (PMU), two irradiation modes can be implemented: (1) pulsed light stimulation (PLS), which provides continuous low-dose irradiation and is suitable for the cleaning of small residual tumors, and (2) intermittent continuous light stimulation (ICLS), which can provide strong radiation intermittently and is suitable for the initial effective killing of tumor tissue. Therefore, a patient can manage the

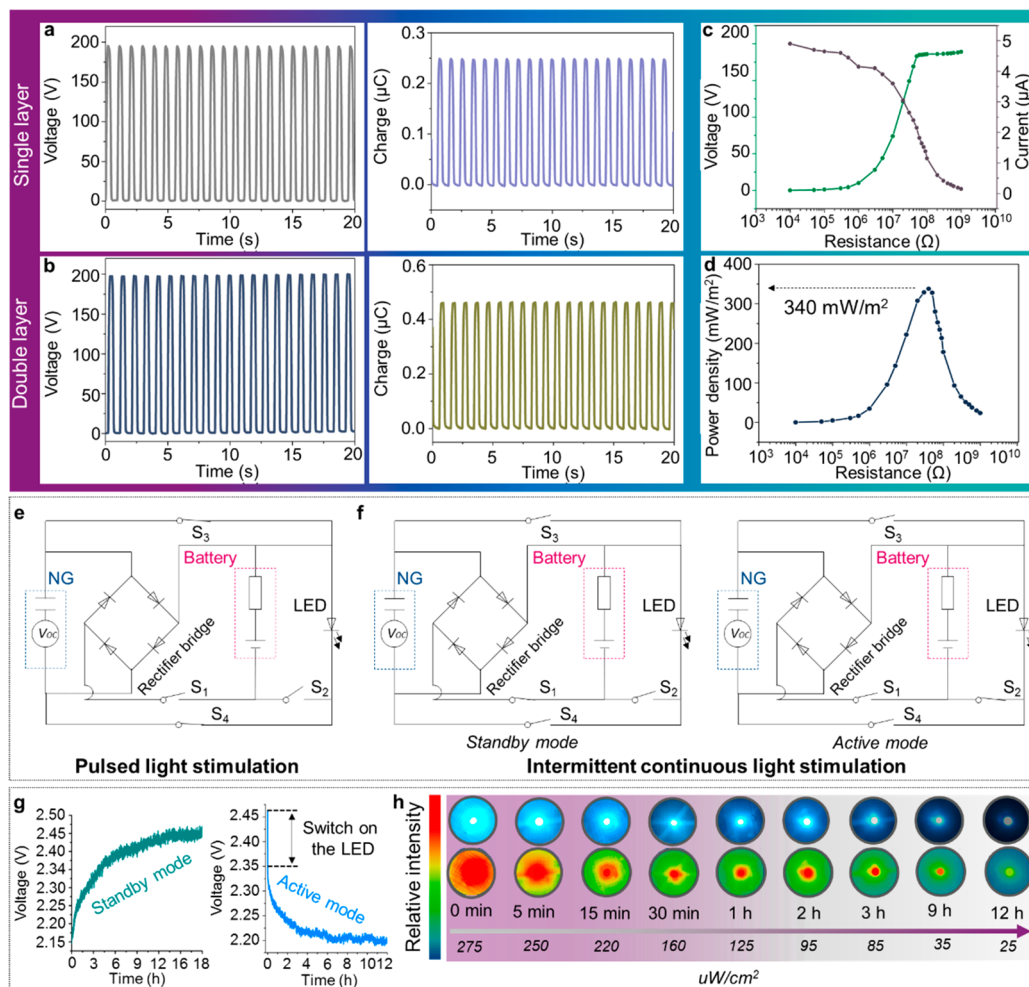


Figure 2. Characterization of energy-harvesting unit. (a) V_{oc} and Q_{sc} of the PENG with a single PVDF layer. (b) V_{oc} and Q_{sc} of the ts-PENG with double PVDF layers. (c,d) Output characteristics of the ts-PENG when connected with different loads from 10 k Ω to 1 G Ω . (e,f) Schematic circuit diagram showing the module of PLS and ICLS. (g) Charging and discharging curve of the button cell by ts-PENG and LED, respectively. (h) Light intensity of LED changing with time.

device autonomously according to different treatment needs and stages, which is ideal for telemedicine scenarios in the future. Specifically, the discontinuous, low-dose PLS stimulation generated by the s-PDT system can significantly control tumor cell growth with a $\sim 60\%$ inhibition rate *in vitro*. The human motion generated electric power can also be stored in the s-PDT system with a miniature LED (m-LED) implanted subcutaneously in mice with intradermally transplanted tumors. The as-produced ICLS showed significant antitumor effects with irradiation for 12 days with an 87.46% inhibition rate. These results demonstrated that the s-PDT system combined with two treatment modes has great potential as wearable/implantable devices for long-term photodynamic therapy, which would be a promising method with good patient compliance for clinical cancer treatment and future teletherapy.

RESULTS AND DISCUSSION

Overview of the s-PDT System. The s-PDT system consists of a ts-PENG-based energy-harvesting unit, PMU, m-LED, and photosensitizer (PS) (Figure 1a). The ts-PENG converts biomechanical energy from body motion into electrical energy. By controlling the on/off state of switches of PMU, ICLS and PLS are obtained. Figure 1b shows the 3D

structure of the energy harvester unit composed of an encapsulation layer (Parylene-C and ultrathin polyethylene terephthalate, PET), the substrate (PET), double piezoelectric layer (poly(vinylidene fluoride), PVDF), and silver (Ag) electrodes. Copper (Cu) tape is employed to fix the lead wire with electrode layers. The apoptotic process of subcutaneous tumor tissue treated by the s-PDT system is presented in Figure 1c. According to the cross-sectional scanning electron microscopy (SEM) image of the energy harvester unit (Figure 1d), the twining structure of the device was revealed clearly. The overall size of the device is 2 cm \times 6 cm \times 0.5 mm (Figure 1e,f), and the weight is just about 1.68 g (Figure 1g). Therefore, the device with characteristics of light weight and flexibility can be attached easily on the body to harvest biomechanical energy. The crystal structure of PVDF film was characterized by Fourier transform infrared (FTIR) measurement. From the data shown in Figure S1, the characteristic absorption bands at 840 and 1430 cm^{-1} are associated with a β -phase structure. The main working mode of the PVDF is d_{31} , which means the force applied to a material is perpendicular to the direction of the polarization electric field (Figure 1h). The working principle of the PENG is presented in Figure 1i. In detail, the electric dipole in PVDF is arranged along the direction of the top and bottom electrodes

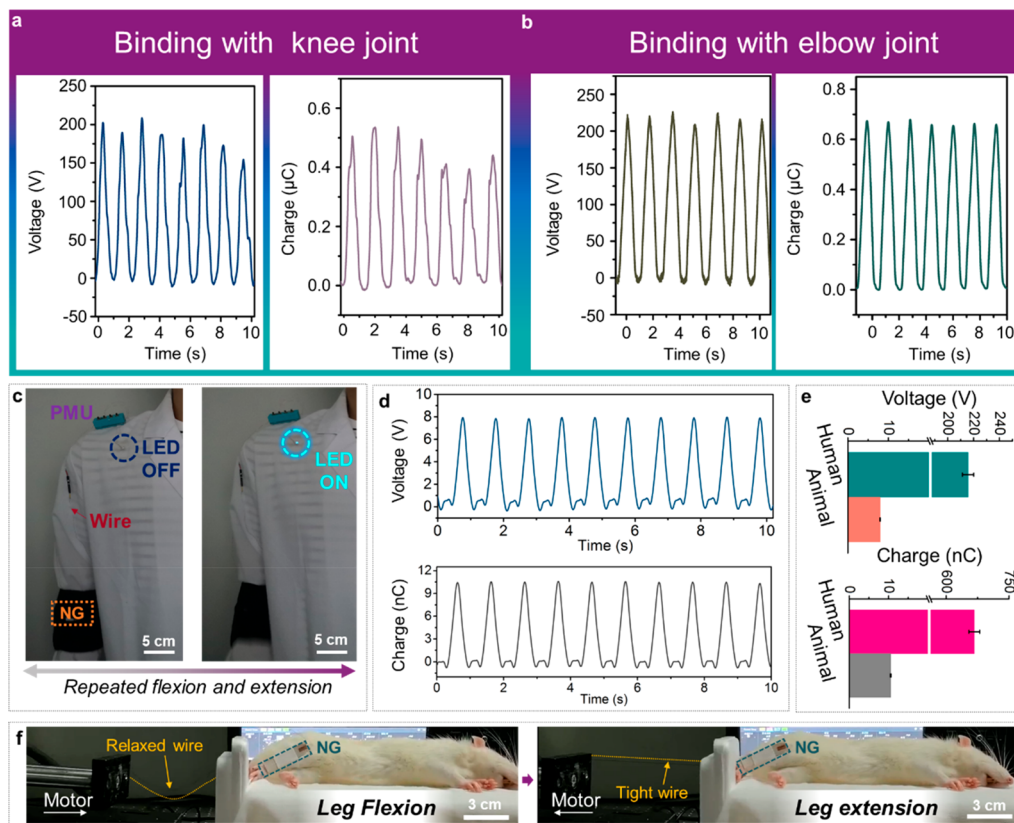


Figure 3. Output performance of wearable ts-PENG from human to animal. (a) V_{oc} and Q_{sc} of the ts-PENG binding with the knee joint. (b) V_{oc} and Q_{sc} of the ts-PENG binding with the elbow joint. (c) LED lighted by the wearable ts-PENG system (the size of PMU is 1.7 cm \times 4.8 cm \times 1.3 cm). (d) V_{oc} and Q_{sc} of the smaller ts-PENG on animal body. (e) Statistical comparison of average V_{oc} of the ts-PENG on the human body and an animal body. (f) Animal model test system.

when mechanical deformation is applied in the direction of the vertical device. The PVDF generates a piezoelectric polarization charge, and generated electric field attracts/repulses electrons in the upper and lower electrodes. When an external load circuit is connected, electrons flow from one electrode to the other electrode. When the external mechanical force is removed, the electric field generated by piezoelectric polarization charge disappears, and electrons flow in the opposite direction through the external load.

Characterization of the Energy-Harvesting Unit. To enhance the output performance of the energy-harvesting unit for realizing efficient energy conversion, we designed the ts-PENG and systematically investigated the effect of the double PVDF layers on the output performance of the energy-harvesting unit by applying a periodic external mechanical force. For a single PVDF layer, the open-circuit voltage (V_{oc}) and short-circuit transferred charge (Q_{sc}) are about 200 V and 0.25 μC , respectively (Figure 2a). After the double PVDF layers were attached on the front and back of the substrate layer (PET) with parallel connection as a twinning structure ts-PENG, the V_{oc} and Q_{sc} reached ~ 200 V and ~ 0.46 μC , respectively (Figure 2b). The Q_{sc} of the ts-PENG is enhanced by 2-fold. The peak power density of ts-PENG can reach 340 mW/m^2 by monitoring the V_{oc} and short-circuit current (I_{sc}) with variable load resistances ranging from 10 $\text{k}\Omega$ to 10 $\text{G}\Omega$ (Figure 2c,d). By controlling the on/off state of the switches of PMU, PLS (Figure 2e) and ICLS (Figure 2f) are obtained. When turning off switches 1 and 2 and turning on switches 3 and 4, the ts-PENG can be directly connected with the m-LED

and generate PLS (Figure S2a, Supporting Information), of which the blinking rhythm is consistent with the frequency of applied mechanical stimulation. If switches 2–4 are turned off and switch 1 is turned on, the electrical energy can be stored in the button cell through the rectifier bridge (standby mode). When enough energy has been stored, the active module starts (switches 1, 3, 4 off, switch 2 on) to power the load (LED). This alternating charge and discharge process is called the ICLS mode (Figure S2b, Supporting Information). In addition, these modes can be integrated as a wearable system (Figure S2c,d, Supporting Information). A button cell is charged by the ts-PENG from 2.15 to 2.47 V in 18 h and discharged by the LED load from 2.47 to 2.18 V in 12 h (Figure 2g). The maximum intensity is about 275 $\mu\text{W}/\text{cm}^2$, and after 12 h of LED operation, the light intensity can still reach 25 $\mu\text{W}/\text{cm}^2$ (Figure 2h).

Output Performance of Wearable ts-PENG from Humans to Animals. To evaluate the possibility of wearable self-powered photodynamic therapy system, we attached the ts-PENG to the knee joint and the elbow joint of a human and tested the V_{oc} and Q_{sc} of the ts-PENG on these two positions, respectively. Binding with the knee joint, the V_{oc} and Q_{sc} of the PENG are about 200 V and 0.5 μC , respectively (Figure 3a and Video S1, Supporting Information). In contrast to the knee joint, when binding with the elbow joint, the V_{oc} and Q_{sc} of the ts-PENG can reach 220 V and 0.65 μC , respectively (Figure 3b and Video S2, Supporting Information). Based on the above results, the output performance of the ts-PENG driven by human joint motion is approximately the same as

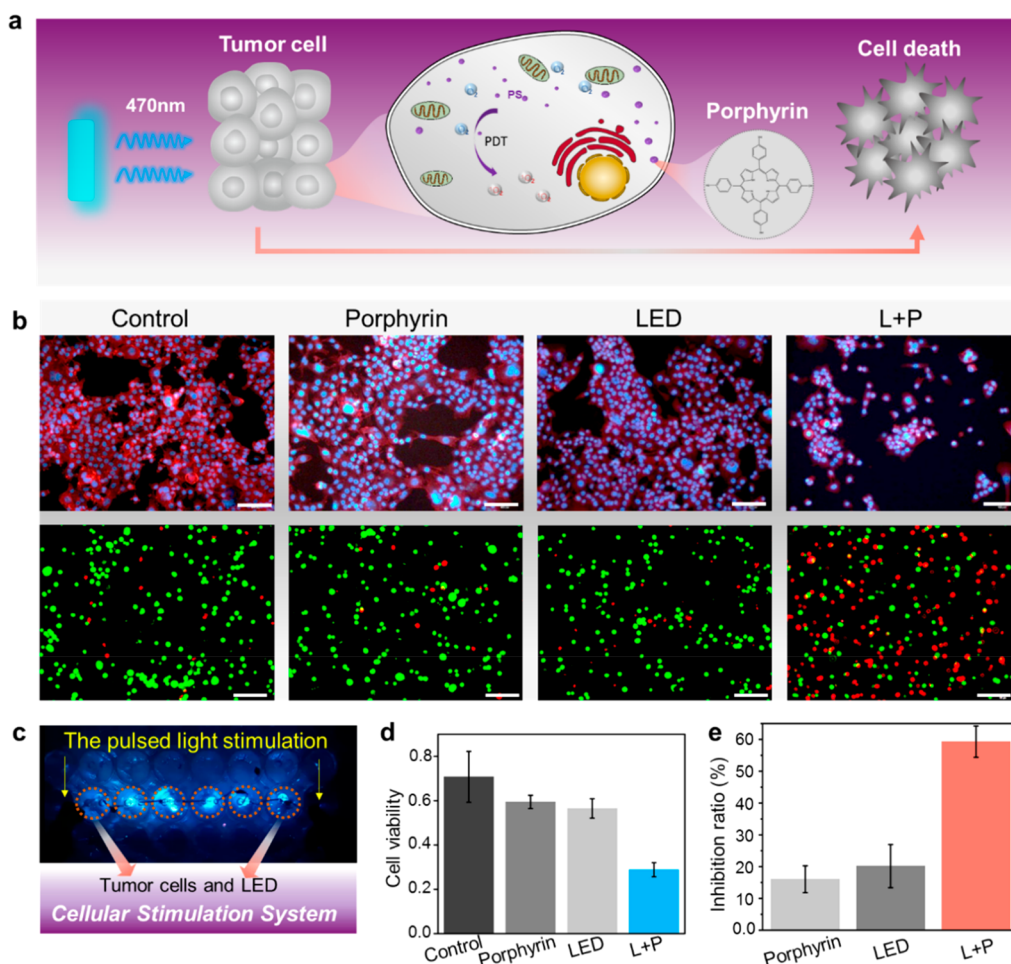


Figure 4. Pulsed light stimulation for treating the tumor cells *in vitro*. (a) Mechanism of action of PDT. (b) Fluorescence images (cytoskeleton and cell nucleus, scale bar = 100 μm ; live and dead cells, scale bar = 200 μm) of stained 4T1 cells in the different groups. (c) Image of the cellular stimulation system. (d) Cell viability in the different groups. (e) Inhibition ratio in the different groups.

applying a periodic external mechanical force by a linear motor; in addition, the LED can be driven directly by the wearable ts-PENG (Figure 3c). It shows that the PLS and ICLS can be realized on the human body (Video S3 Supporting Information). The V_{oc} of the ts-PENG remained stable in comparison with its initial state after 1 million working cycles (Figure S3, Supporting Information), exhibiting good durability. We also studied the relationship between the output performance of the ts-TENG and the bend angle of the elbow joint (Figure S4, Supporting Information). The V_{oc} of ts-PENG is positively correlated with the bending angle, and the ts-PENG with small amplitude motion can also get good output performance, which is applied to different forms of joint movement in daily life.

Considering that the tumor model is constructed in mice, the smaller ts-PENG is attached to the leg of a rat and the linear motor is employed to pull the leg to simulate body motion. The animal model test system is shown in Figure 3f. The output performance of ts-PENG on a rat body with a size of 1 cm \times 4 cm is also evaluated. The outputs V_{oc} and Q_{sc} are typically about 8 V and 10.5 nC, respectively (Figure 3d). The output performance of ts-PENG is declined dozens of times from the human body to the small animal body (Figure 3e). The output performance of ts-PENG is rather weak due to the restricted size and the magnitude of movement of a rat, which did not satisfy the therapy in a smaller animal model.

Therefore, we proposed a compromise using a line motor to drive the ts-PENG to simulate human movement to power a LED directly or charge a button cell *via* PMU. It means that the output power level of the ts-PENG from the human body is employed to treat the tumor cell *in vitro* and the tumor *in vivo*. The energy source of the entire system is the conversion of biomechanical energy into electrical energy by the ts-PENG during the treatment process.

Pulsed Light Stimulation for Treating the Tumor Cell *in Vitro*. Given the feasibility of the pulsed light stimulation for the cleaning of small residual tumors, we demonstrate the effect of the s-PDT system at the cellular level. The LED with 470 nm emission wavelength is directly driven by ts-PENG, which is employed to stimulate the 4T1 tumor cells as an illuminant. A blue light source with higher energy is harmful to both mice and human skin under normal conditions. However, for our study, we use a breast tumor cell model, and our treatment method is to implant a light source subcutaneously, which requires less penetration, shorter wavelength, and higher single-photon energy. Depending on the type of tissue, the penetration depth is less than 1 mm at 400 nm, 0.5 to 2 mm at 514 nm, and up to 6 mm at 630 nm.⁴⁷ The 470 nm spectrum width has a greater ability to penetrate the skin compared to the 400 nm spectrum and provides more efficient porphyrin photosensitization than the red-light spectrum. The mechanism of PDT is shown in Figure 4a. The porphyrin is a PS

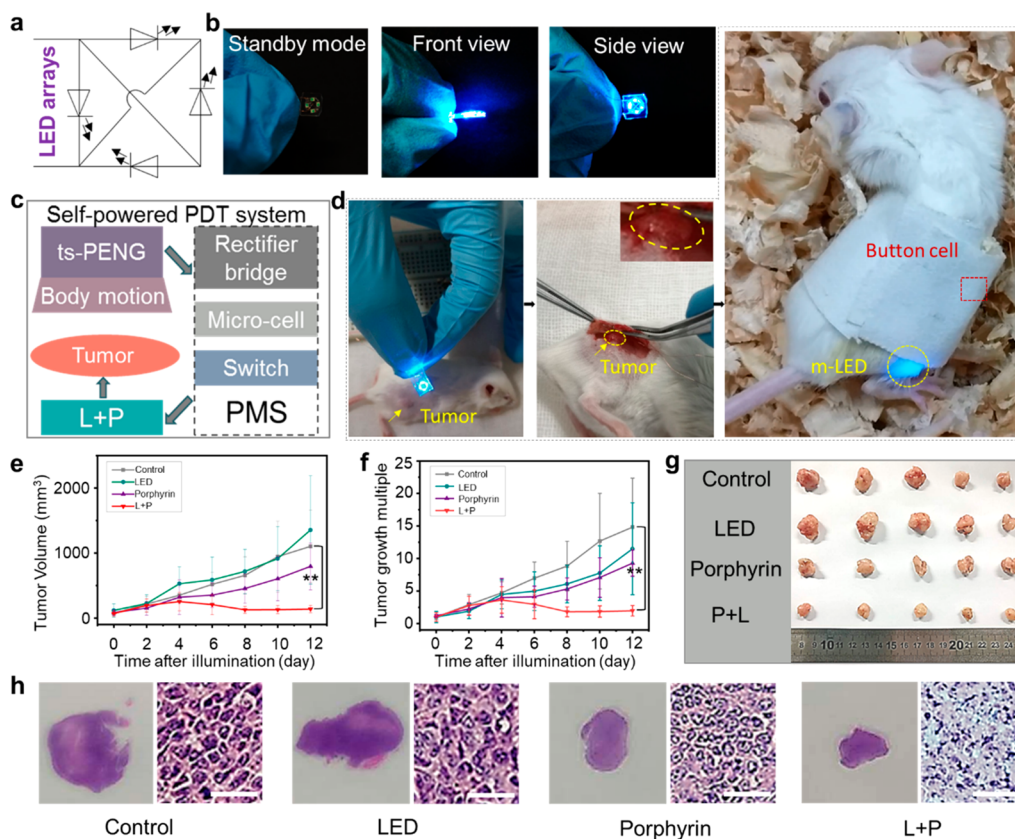


Figure 5. Intermittent continuous light stimulation for treating the tumor *in vivo*. (a) Circuit diagram of the LED arrays. (b) Image of LED arrays encapsulated by PDMS in different states and views. (c) Diagram of the components in the s-PDT system. (d) Process of tumor model and s-PDT system construction on the animal. (e) Tumor volume of different experimental groups in 12 days. (f) Tumor growth multiplication of different experimental groups in 12 days. (g,h) Image of the tumors and pathological section (scale bar = 50 μm) in different experimental groups after 12 days.

transfer the energy from LED. 4T1 tumor cells are cultured with porphyrin, LED, and LED + porphyrin. The absorption spectrum of porphyrin is shown in Figure S5, and porphyrin has an absorption at 470 nm, which is stronger than that at 660 nm. The blank control group did not do any treatment. Two days after incubation, we applied the stimulation for 24 h. Fluorescence images (cytoskeleton and cell nucleus, live and dead cells) of stained 4T1 cells in the different groups are shown in Figure 4b and Figure S6. The cell number of the experimental group from LED + porphyrin is significantly less than that in other groups. In addition, The LED + porphyrin experimental group has the highest percentage of dead cells. The image of the cellular stimulation system is shown in Figure 4c, and the linear motor is employed to drive the ts-PENG to simulate human movement (Video S4, Supporting Information). After statistical analysis based on the 3-(4,5-dimethylthiazol-2-yl)-2,5-diphenyltetrazolium bromide (MTT) absorbance value, the cell viability of each group is shown in Figure 4d, and the inhibition ratio in different groups is shown in Figure 4e, which demonstrates that the s-PDT system based on pulsed light stimulation can significantly control tumor cell growth with $\sim 60\%$ inhibition rate.

Intermittent Continuous Light Stimulation for Treating the Tumor *in Vivo*. The antitumor efficiency of the s-PDT system based on the ts-PENG and power management unit is further investigated *in vivo*. The m-LED arrays are encapsulated by polydimethylsiloxane (PDMS) with a size of 5 mm \times 5 mm, and the thickness is only 1 mm. Figure 5a

presents the circuit diagram of the LED arrays. The image of LED arrays encapsulated by PDMS with good biocompatibility in different states and view is shown in Figure 5b. The illuminant is implanted *in vivo* to adjoin the tumor location. The diagram of the components in the s-PDT system is shown in Figure 5c. In detail, first, the ts-PENG converts biomechanical energy generated by body motion into electrical energy. Then, the electric energy is stored in the button cell *via* a rectifier bridge. The s-PDT system charging and discharging are controlled by switches. The rectifier bridge, button cell, and switches are called the PMU. Finally, the m-LED could be powered by the PMU to stimulate porphyrin to realize the s-PDT. A BALB/c mouse was used as the animal model. The construction process of the tumor model and the s-PDT system on animals is shown in Figure 5d and Video S5. The tumor is inoculated on the upper thigh of the mouse by directly injecting 4T1 cells. The changes in the tumor volume over time in different experiment groups are shown in Figure 5e. The tumor volume of each group before stimulation is defined as a fiducial value, hence, the tumor growth multiple of different experiment groups in 12 days is shown in Figure 5f. The tumor in the experimental group (LED + porphyrin) has obvious inhibition after 12 days, and the volume of the tumor remained stable compared to the other three groups. On day 12, the mice of each group were sacrificed and the tumors were collected, as shown in Figure 5g. Tumors in the LED + porphyrin group have a volume significantly smaller than that in the other groups, which shows significant antitumor effects

by intermittent continuous light stimulation with 87.46% inhibition rate. A hematoxylin/eosin (H&E) staining picture of tissues of different groups on day 12 are shown in Figure 5h. The viable cancer cells in three control groups (control, LED, porphyrin) filled in the residual tumor and showed the typical characteristics of cancer with large and prominent nuclei, irregular shape, and scanty cytoplasm. On the contrary, the nuclei of the experimental group (LED + porphyrin) were collapsed and wizened, which revealed the cellular state of the experimental group (LED + porphyrin) is much worse than that in the control group. These results demonstrate that the antitumor effect was probably due to the s-PDT system at the tumor site.

CONCLUSION

In summary, we have designed a self-powered PDT system based on ts-PENG with good biocompatibility and flexibility. The ts-PENG can be utilized as a wearable and implantable power source for converting biomechanical energy from body motion into electricity. The output performance of ts-PENG is influenced by many factors, mainly including the size of the device as well as the magnitude of the stress and strain. Through a well-designed power management unit, two irradiation modes (PLS and ICLS) can be well adapted to the treatment of different tumor progression. This strategy suggests that our approach is feasible in future clinical applications, which will bring an effective therapeutic strategy for cancer treatment. Our research may also provide an inspiration for creating self-powered wearable/implantable electronic systems for various disease requiring long-term treatment, like diabetes, Parkinson's disease, or cardiovascular disease, which has great potential for clinical applications.

EXPERIMENTAL SECTION

Fabrication of ts-PENG. The PENG was composed of a piezoelectric layer, electrodes, elastic substrate, and an encapsulation layer. PET (2 cm × 6 cm × 100 μm) was used as the substrate; PVDF film covered with silver (1.8 cm × 5.8 cm × 110 μm) was adopted as the piezoelectric layer, and silver was the electrode. Two piezoelectric layers were attached on both sides of the PET. The copper tape was used to fix lead on the piezoelectric layers. The ultrathin PET film (2 cm × 6 cm × 20 μm) was employed as a package layer on the surface of PVDF film. All parts were glued together *via* silicone polymers one by one. After being dried naturally, Parylene-C was deposited on the surface of the device with the parylene coating system (PDS2010 Labcoater2).

Characterization Methods. The SEM image was taken with a Hitachi cold field emission scanning electron microscope (SU8020). The voltage, current, and transferred charge were detected by an electrometer (Keithley 6517B) and recorded by an oscilloscope (Teledyne LeCroy HD 4096). The fluorescence staining photographs of the tumor cells were taken with an inversion fluorescence microscope (Olympus IX71). When the LED was lit, the optical power meter (Q8320 ADCMT) was placed ~1 mm above the lamp to measure the light intensity, and photos were taken at the same time in the all-black environment. Photographs were processed by ImageJ to simulate the relative intensity.

Output Characterization of ts-PENG. ts-PENG was driven by a linear motor (frequency, acceleration, deceleration, speed, and adjustable operation distance). The wires of the ts-PENG were connected with an electrometer and recorded by an oscilloscope to acquire electric signals.

Wearable System Verification. For humans, the ts-PENG was fixed on the elbow joint and knee joint of the experimenter, and the open-circuit voltage and transferred charge were measured during normal walking. For animals, the animal model we used was a

Sprague-Dawley rat (~200 g); after anesthesia, the ts-PENG (1 cm × 4 cm × 500 μm) of the same structure was fixed on the elbow of the rat with medical tape. The claws of the rat were connected to the linear motors *via* a wire to control the leg flexion and extension. The voltage and transferred charge were detected.

Photodynamic Therapy *in Vitro*. LED as the stimulating light source (blue LEDs: wavelength 470 nm) for each well of a 48-well plate was produced specifically for *in vitro* PDT. 4T1 cells (400 μL, 5 × 10⁴ cells/mL) were seed in the plate and placed in an incubator under the standard culture conditions. After 36 h, 12 μL of porphyrin was added in the concentration of 100 μg/mL. Twelve hours later, the blue LED was driven by a linear motor that directly lighted six LEDs, and the position of the LED was in the right above of the medium, close but not touching. After 24 h of irradiation, cell viability was determined using the MTT assay. Sample absorbance was read on a Microplate reader (Thermo Scientific, USA) at 570 nm. Calcein-AM and propidium iodide (Invitrogen USA) were used for live/dead staining. The cytoskeletons and nuclei of the cells were stained with phalloidin and 4',6-diamidino-2-phenylindole (DAPI), respectively.

LED Array Design and Fabrication. The LED array consists of four LEDs (Kingbright, 1.6 × 0.8 mm × 0.75 mm) connected in parallel. An encapsulating layer of PDMS by spin-casting and curing at 70 °C for 1 h.

Photodynamic Therapy *in Vivo*. Female BALB/c mice aged at 6–8 weeks were used as the model. 4T1 tumor cells (0.1 mL, 1 × 10⁷ cells/mL) were inoculated in the thigh of the mouse. When the tumor volume reached 100 mm³, the animals were randomly divided into four groups (*n* = 5 per group): (i) control untreated; (ii) administered with porphyrin; (iii) implanted with functional chip LED array; (iv) treatment group implanted with a functional LED array and administered with porphyrin. Forty-five micrograms of porphyrin was injected into mice *in situ*, and the chip LED array was implanted 1 day later. The chip LED array was driven by a button battery, and the battery was changed every 12 h. After the mice were sacrificed, the tumors were removed and kept in 10% formalin at 4 °C followed by being embedded in paraffin and sectioned into slides. Slides were stained with H&E to observe the morphology. All of the animal experiments were performed strictly in accordance with "Beijing Administration Rule of Laboratory Animals" and the national standard "Laboratory Animal Requirements of Environment and Housing Facilities (GB 14925-2001)".

Statistical Analysis. The data were presented as the mean ± SD (standard deviation), with a group size of *n* ≥ 5. A two-tailed unpaired *t* test was used to calculate the *p* values. Statistical significance was accepted at **p* < 0.05, ***p* < 0.01, and ****p* < 0.001.

ASSOCIATED CONTENT

Supporting Information

The Supporting Information is available free of charge at <https://pubs.acs.org/doi/10.1021/acsnano.0c00675>.

Detailed data and images of FTIR spectra of the PVDF film, circuit control diagram of two different irradiation modes, fatigue performance of the ts-PENG, relationship between the output performance of the ts-TENG and bend angle, absorption spectrum of porphyrin, fluorescence images of nuclear and cytoskeletal staining in different groups of 4T1 (PDF)

Video S1: Output of ts-PENG binding with a human knee joint (MP4)

Video S2: Output of ts-PENG binding with a human elbow joint (MP4)

Video S3: PLS and ICLS realized on the human body (MP4)

Video S4: Linear motor simulates human motion to drive the ts-PENG (MP4)

Video S5: s-PDT system on a BALB/c mouse (MP4)

AUTHOR INFORMATION

Corresponding Authors

Yubo Fan – Beijing Advanced Innovation Centre for Biomedical Engineering, Key Laboratory for Biomechanics and Mechanobiology of Ministry of Education, School of Biological Science and Medical Engineering, Beihang University, Beijing 100083, China; National Research Center for Rehabilitation Technical Aids, Beijing 100176, China; Email: yubofan@buaa.edu.cn

Zhong Lin Wang – CAS Center for Excellence in Nanoscience, Beijing Key Laboratory of Micro-nano Energy and Sensor, Beijing Institute of Nanoenergy and Nanosystems, Chinese Academy of Sciences, Beijing 100083, China; School of Nanoscience and Technology, University of Chinese Academy of Sciences, Beijing 100049, China; School of Materials Science and Engineering, Georgia Institute of Technology, Atlanta, Georgia 30332, United States; orcid.org/0000-0002-5530-0380; Email: zhong.wang@mse.gatech.edu

Zhou Li – CAS Center for Excellence in Nanoscience, Beijing Key Laboratory of Micro-nano Energy and Sensor, Beijing Institute of Nanoenergy and Nanosystems, Chinese Academy of Sciences, Beijing 100083, China; School of Nanoscience and Technology, University of Chinese Academy of Sciences, Beijing 100049, China; orcid.org/0000-0002-9952-7296; Email: zli@binn.cas.cn

Authors

Zhuo Liu – CAS Center for Excellence in Nanoscience, Beijing Key Laboratory of Micro-nano Energy and Sensor, Beijing Institute of Nanoenergy and Nanosystems, Chinese Academy of Sciences, Beijing 100083, China; Beijing Advanced Innovation Centre for Biomedical Engineering, Key Laboratory for Biomechanics and Mechanobiology of Ministry of Education, School of Biological Science and Medical Engineering, Beihang University, Beijing 100083, China

Lingling Xu – CAS Center for Excellence in Nanoscience, Beijing Key Laboratory of Micro-nano Energy and Sensor, Beijing Institute of Nanoenergy and Nanosystems, Chinese Academy of Sciences, Beijing 100083, China; School of Nanoscience and Technology, University of Chinese Academy of Sciences, Beijing 100049, China

Qiang Zheng – CAS Center for Excellence in Nanoscience, Beijing Key Laboratory of Micro-nano Energy and Sensor, Beijing Institute of Nanoenergy and Nanosystems, Chinese Academy of Sciences, Beijing 100083, China; School of Nanoscience and Technology, University of Chinese Academy of Sciences, Beijing 100049, China

Yong Kang – School of Nanoscience and Technology, University of Chinese Academy of Sciences, Beijing 100049, China; State Key Laboratory of Biochemical Engineering, Institute of Process Engineering, Chinese Academy of Sciences, Beijing 100190, China

Bojing Shi – CAS Center for Excellence in Nanoscience, Beijing Key Laboratory of Micro-nano Energy and Sensor, Beijing Institute of Nanoenergy and Nanosystems, Chinese Academy of Sciences, Beijing 100083, China; Beijing Advanced Innovation Centre for Biomedical Engineering, Key Laboratory for Biomechanics and Mechanobiology of Ministry of Education, School of Biological Science and Medical Engineering, Beihang University, Beijing 100083, China

Dongjie Jiang – CAS Center for Excellence in Nanoscience, Beijing Key Laboratory of Micro-nano Energy and Sensor, Beijing Institute of Nanoenergy and Nanosystems, Chinese

Academy of Sciences, Beijing 100083, China; School of Nanoscience and Technology, University of Chinese Academy of Sciences, Beijing 100049, China

Hu Li – CAS Center for Excellence in Nanoscience, Beijing Key Laboratory of Micro-nano Energy and Sensor, Beijing Institute of Nanoenergy and Nanosystems, Chinese Academy of Sciences, Beijing 100083, China; Beijing Advanced Innovation Centre for Biomedical Engineering, Key Laboratory for Biomechanics and Mechanobiology of Ministry of Education, School of Biological Science and Medical Engineering, Beihang University, Beijing 100083, China

Xuecheng Qu – CAS Center for Excellence in Nanoscience, Beijing Key Laboratory of Micro-nano Energy and Sensor, Beijing Institute of Nanoenergy and Nanosystems, Chinese Academy of Sciences, Beijing 100083, China; School of Nanoscience and Technology, University of Chinese Academy of Sciences, Beijing 100049, China

Complete contact information is available at:

<https://pubs.acs.org/10.1021/acsnano.0c00675>

Author Contributions

[#]Z. Liu, L.X., and Q.Z. contributed equally to this work.

Notes

The authors declare no competing financial interest.

ACKNOWLEDGMENTS

This study was supported by the National Key R&D project from Minister of Science and Technology, China (2016YFA0202703), National Natural Science Foundation of China (Nos. 61875015, 81601629, 21801019, 11421202, and 11827803), the 111 Project (Project No. B13003), the Beijing Natural Science Foundation (7204333), Key-Area Research and Development Program of Guangdong Province (2018B030331001), the University of Chinese Academy of Sciences (Y954019) and the National Youth Talent Support Program.

REFERENCES

- (1) Barretina, J.; Caponigro, G.; Stransky, N.; Venkatesan, K.; Margolin, A. A.; Kim, S.; Wilson, C. J.; Lehar, J.; Kryukov, G. V.; Sonkin, D.; Reddy, A.; Liu, M.; Murray, L.; Berger, M. F.; Monahan, J. E.; Morais, P.; Meltzer, J.; Korejwa, A.; Jane-Valbuena, J.; Mapa, F. A.; et al. The Cancer Cell Line Encyclopedia Enables Predictive Modelling of Anticancer Drug Sensitivity. *Nature* **2012**, *492*, 290.
- (2) Brown, J. M.; Wilson, W. R. Exploiting Tumour Hypoxia in Cancer Treatment. *Nat. Rev. Cancer* **2004**, *4*, 437–447.
- (3) Piccart-Gebhart, M. J.; Procter, M.; Leyland-Jones, B.; Goldhirsch, A.; Untch, M.; Smith, I.; Gianni, L.; Baselga, J.; Bell, R.; Jackisch, C.; Cameron, D.; Dowsett, M.; Barrios, C. H.; Steger, G.; Huang, C. S.; Andersson, M.; Inbar, M.; Lichinitser, M.; Lang, I.; Nitz, U.; et al. Trastuzumab after Adjuvant Chemotherapy in HER2-Positive Breast Cancer. *N. Engl. J. Med.* **2005**, *353*, 1659–1672.
- (4) Dolmans, D. E. J. G. J.; Fukumura, D.; Jain, R. K. Photodynamic Therapy for Cancer. *Nat. Rev. Cancer* **2003**, *3*, 380–387.
- (5) Celli, J. P.; Spring, B. Q.; Rizvi, I.; Evans, C. L.; Samkoe, K. S.; Verma, S.; Pogue, B. W.; Hasan, T. Imaging and Photodynamic Therapy: Mechanisms, Monitoring, and Optimization. *Chem. Rev.* **2010**, *110*, 2795–2838.
- (6) Castano, A. P.; Mroz, P.; Hamblin, M. R. Photodynamic Therapy and Anti-Tumour Immunity. *Nat. Rev. Cancer* **2006**, *6*, 535–545.
- (7) Moore, C. M.; Pendse, D.; Emberton, M. Photodynamic Therapy for Prostate Cancer—A Review of Current Status and Future Promise. *Nat. Clin. Pract. Urol.* **2009**, *6*, 18–30.

- (8) Kopelman, R.; Lee Koo, Y.-E.; Philbert, M.; Moffat, B. A.; Ramachandra Reddy, G.; McConville, P.; Hall, D. E.; Chenevert, T. L.; Bhojani, M. S.; Buck, S. M.; Rehemtulla, A.; Ross, B. D. Multifunctional Nanoparticle Platforms for *In Vivo* MRI Enhancement and Photodynamic Therapy of a Rat Brain Cancer. *J. Magn. Mater.* **2005**, *293*, 404–410.
- (9) Wieder, M. E.; Hone, D. C.; Cook, M. J.; Handsley, M. M.; Gavrilovic, J.; Russell, D. A. Intracellular Photodynamic Therapy with Photosensitizer-Nanoparticle Conjugates: Cancer Therapy Using a ‘Trojan Horse’. *Photochem. Photobiol. Sci.* **2006**, *5*, 727–34.
- (10) Ohulchanskyy, T. Y.; Roy, I.; Goswami, L. N.; Chen, Y.; Bergey, E. J.; Pandey, R. K.; Oseroff, A. R.; Prasad, P. N. Organically Modified Silica Nanoparticles with Covalently Incorporated Photosensitizer for Photodynamic Therapy of Cancer. *Nano Lett.* **2007**, *7*, 2835–42.
- (11) Lukyanets, E. A. Phthalocyanines as Photosensitizers in the Photodynamic Therapy of Cancer. *J. Porphyrins Phthalocyanines* **1999**, *3*, 424–432.
- (12) Chen, W. R.; Adams, R. L.; Carubelli, R.; Nordquist, R. E. Laser-Photosensitizer Assisted Immunotherapy: A Novel Modality for Cancer Treatment. *Cancer Lett.* **1997**, *115*, 25–30.
- (13) Dolmans, D. E. J. G. J.; Kadambi, A.; Hill, J. S.; Flores, K. R.; Gerber, J. N.; Walker, J. P.; Rinkes, I. H. M. B.; Jain, R. K.; Fukumura, D. Targeting Tumor Vasculature and Cancer Cells in Orthotopic Breast Tumor by Fractionated Photosensitizer Dosing Photodynamic Therapy. *Cancer Res.* **2002**, *62*, 4289–4294.
- (14) Dougherty, T. J.; Marcus, S. L. Photodynamic Therapy. *Eur. J. Cancer* **1992**, *28a*, 1734–1742.
- (15) MacDonald, I. J.; Dougherty, T. J. Basic Principles of Photodynamic Therapy. *J. Porphyrins Phthalocyanines* **2001**, *5*, 105–129.
- (16) Mackenzie, G. D.; Jamieson, N. F.; Novelli, M. R.; Mosse, C. A.; Clark, B. R.; Thorpe, S. M.; Bown, S. G.; Lovat, L. B. How Light Dosimetry Influences the Efficacy of Photodynamic Therapy with 5-Aminolaevulinic Acid for Ablation of High-Grade Dysplasia in Barrett’s Esophagus. *Laser Med. Sci.* **2008**, *23*, 203–210.
- (17) Kinsey, J. H.; Cortese, D. A.; Neel, H. B. Thermal Considerations in Murine Tumor Killing Using Hematoporphyrin Derivative Phototherapy. *Cancer Res.* **1983**, *43*, 1562–1567.
- (18) Horimatsu, T.; Muto, M.; Yoda, Y.; Yano, T.; Ezoe, Y.; Miyamoto, S.; Chiba, T. Tissue Damage in the Canine Normal Esophagus by Photoactivation with Talaporfin Sodium (Laserphyrin): A Preclinical Study. *PLoS One* **2012**, *7*, No. e38308.
- (19) Seshadri, M.; Bellnier, D. A.; Vaughan, L. A.; Spornyak, J. A.; Mazurchuk, R.; Foster, T. H.; Henderson, B. W. Light Delivery over Extended Time Periods Enhances the Effectiveness of Photodynamic Therapy. *Clin. Cancer Res.* **2008**, *14*, 2796–2805.
- (20) Wang, J. H.; He, H.; Xu, X.; Wang, X.; Chen, Y. B.; Yin, L. C. Far-Red Light-Mediated Programmable Anti-Cancer Gene Delivery in Cooperation with Photodynamic Therapy. *Biomaterials* **2018**, *171*, 72–82.
- (21) Bisland, S. K.; Lilge, L.; Lin, A.; Rusnov, R.; Wilson, B. C. Metronomic Photodynamic Therapy as a New Paradigm for Photodynamic Therapy: Rationale and Preclinical Evaluation of Technical Feasibility for Treating Malignant Brain Tumors. *Photochem. Photobiol.* **2004**, *80*, 22–30.
- (22) van Zaane, F.; Subbaiyan, D.; van der Ploeg-van den Heuvel, A.; de Bruijn, H. S.; Margallo Balbas, E.; Pandraud, G.; Sterenborg, H. J. C. M.; French, P. J.; Robinson, D. J. A Telemetric Light Delivery System for Metronomic Photodynamic Therapy (mPDT) in Rats. *J. Biophotonics* **2010**, *3*, 347–355.
- (23) Yamagishi, K.; Kirino, I.; Takahashi, I.; Amano, H.; Takeoka, S.; Morimoto, Y.; Fujie, T. Tissue-Adhesive Wirelessly Powered Optoelectronic Device for Metronomic Photodynamic Cancer Therapy. *Nat. Biomed. Eng.* **2019**, *3*, 27–36.
- (24) Fan, F. R.; Tian, Z. Q.; Wang, Z. L. Flexible Triboelectric Generator! *Nano Energy* **2012**, *1*, 328–334.
- (25) Wang, Z. L.; Song, J. H. Piezoelectric Nanogenerators Based on Zinc Oxide Nanowire Arrays. *Science* **2006**, *312*, 242–246.
- (26) Wang, J.; Li, S. M.; Yi, F.; Zi, Y. L.; Lin, J.; Wang, X. F.; Xu, Y. L.; Wang, Z. L. Sustainably Powering Wearable Electronics Solely by Biomechanical Energy. *Nat. Commun.* **2016**, *7*, 12744.
- (27) Wang, Z. L. Catch Wave Power in Floating Nets. *Nature* **2017**, *542*, 159–160.
- (28) Yi, F.; Wang, X. F.; Niu, S. M.; Li, S. M.; Yin, Y. J.; Dai, K. R.; Zhang, G. J.; Lin, L.; Wen, Z.; Guo, H. Y.; Wang, J.; Yeh, M. H.; Zi, Y. L.; Liao, Q. L.; You, Z.; Zhang, Y.; Wang, Z. L. A Highly Shape-Adaptive, Stretchable Design Based on Conductive Liquid for Energy Harvesting and Self-Powered Biomechanical Monitoring. *Sci. Adv.* **2016**, *2*, No. e1501624.
- (29) Wu, W. Z.; Wang, L.; Li, Y. L.; Zhang, F.; Lin, L.; Niu, S. M.; Chenet, D.; Zhang, X.; Hao, Y. F.; Heinz, T. F.; Hone, J.; Wang, Z. L. Piezoelectricity of Single-Atomic-Layer MoS₂ for Energy Conversion and Piezotronics. *Nature* **2014**, *514*, 470–474.
- (30) Chen, B.; Yang, Y.; Wang, Z. L. Scavenging Wind Energy by Triboelectric Nanogenerators. *Adv. Energy Mater.* **2018**, *8*, 1702649.
- (31) Hinchet, R.; Yoon, H. J.; Ryu, H.; Kim, M. K.; Choi, E. K.; Kim, D. S.; Kim, S. W. Transcutaneous Ultrasound Energy Harvesting Using Capacitive Triboelectric Technology. *Science* **2019**, *365*, 491–494.
- (32) Hwang, G. T.; Park, H.; Lee, J. H.; Oh, S.; Park, K. I.; Byun, M.; Park, H.; Ahn, G.; Jeong, C. K.; No, K.; Kwon, H.; Lee, S. G.; Joung, B.; Lee, K. J. Self-Powered Cardiac Pacemaker Enabled by Flexible Single Crystalline PMN-PT Piezoelectric Energy Harvester. *Adv. Mater.* **2014**, *26*, 4880–4887.
- (33) Liu, Z.; Ma, Y.; Ouyang, H.; Shi, B. J.; Li, N.; Jiang, D. J.; Xie, F.; Qu, D.; Zou, Y.; Huang, Y.; Li, H.; Zhao, C. C.; Tan, P. C.; Yu, M.; Fan, Y. B.; Zhang, H.; Wang, Z. L.; Li, Z. Transcatheter Self-Powered Ultrasensitive Endocardial Pressure Sensor. *Adv. Funct. Mater.* **2019**, *29*, 1807560.
- (34) Ouyang, H.; Tian, J. J.; Sun, G. L.; Zou, Y.; Liu, Z.; Li, H.; Zhao, L. M.; Shi, B. J.; Fan, Y. B.; Fan, Y. F.; Wang, Z. L.; Li, Z. Self-Powered Pulse Sensor for Antidiastole of Cardiovascular Disease. *Adv. Mater.* **2017**, *29*, 1703456.
- (35) Cao, R.; Pu, X.; Du, X.; Yang, W.; Wang, J.; Guo, H.; Zhao, S.; Yuan, Z.; Zhang, C.; Li, C.; Wang, Z. L. Screen-Printed Washable Electronic Textiles as Self-Powered Touch/Esture Tribo-Sensors for Intelligent Human–Machine Interaction. *ACS Nano* **2018**, *12*, 5190–5196.
- (36) Yu, X. E.; Wang, H. L.; Ning, X.; Sun, R. J.; Albadawi, H.; Salomao, M.; Silva, A. C.; Yu, Y.; Tian, L. M.; Koh, A.; Lee, C. M.; Chempakasseril, A.; Tian, P. L.; Pharr, M.; Yuan, J. H.; Huang, Y. G.; Oklu, R.; Rogers, J. A. Needle-Shaped Ultrathin Piezoelectric Microsystem for Guided Tissue Targeting via Mechanical Sensing. *Nat. Biomed. Eng.* **2018**, *2*, 165–172.
- (37) Wang, A. C.; Liu, Z.; Hu, M.; Wang, C. C.; Zhang, X. D.; Shi, B. J.; Fan, Y. B.; Cui, Y. G.; Li, Z.; Ren, K. L. Piezoelectric Nanofibrous Scaffolds as *In Vivo* Energy Harvesters for Modifying Fibroblast Alignment and Proliferation in Wound Healing. *Nano Energy* **2018**, *43*, 63–71.
- (38) Tang, W.; Tian, J. J.; Zheng, Q.; Yan, L.; Wang, J. X.; Li, Z.; Wang, Z. L. Implantable Self-Powered Low-Level Laser Cure System for Mouse Embryonic Osteoblasts Proliferation and Differentiation. *ACS Nano* **2015**, *9*, 7867–7873.
- (39) Hwang, G. T.; Park, H.; Lee, J. H.; Oh, S.; Park, K. I.; Byun, M.; Park, H.; Ahn, G.; Jeong, C. K.; No, K.; Kwon, H.; Lee, S. G.; Joung, B.; Lee, K. J. Self-Powered Cardiac Pacemaker Enabled by Flexible Single Crystalline PMN-PT Piezoelectric Energy Harvester. *Adv. Mater.* **2014**, *26*, 4880–4887.
- (40) Dagdeviren, C.; Yang, B. D.; Su, Y. W.; Tran, P. L.; Joe, P.; Anderson, E.; Xia, J.; Doraiswamy, V.; Dehdashti, B.; Feng, X.; Lu, B. W.; Poston, R.; Khalpey, Z.; Ghaffari, R.; Huang, Y. G.; Slepian, M. J.; Rogers, J. A. Conformal Piezoelectric Energy Harvesting and Storage from Motions of the Heart, Lung, and Diaphragm. *Proc. Natl. Acad. Sci. U. S. A.* **2014**, *111*, 1927–1932.
- (41) Zheng, Q.; Shi, B. J.; Fan, F. R.; Wang, X. X.; Yan, L.; Yuan, W. W.; Wang, S. H.; Liu, H.; Li, Z.; Wang, Z. L. *In Vivo* Powering of

Pacemaker by Breathing-Driven Implanted Triboelectric Nanogenerator. *Adv. Mater.* **2014**, *26*, 5851–5856.

(42) Li, J.; Kang, L.; Long, Y.; Wei, H.; Yu, Y. H.; Wang, Y. H.; Ferreira, C. A.; Yao, G.; Zhang, Z. Y.; Carlos, C.; German, L.; Lan, X. L.; Cai, W. B.; Wang, X. D. Implanted Battery-Free Direct-Current Micro-Power Supply from *In Vivo* Breath Energy Harvesting. *ACS Appl. Mater. Interfaces* **2018**, *10*, 42030–42038.

(43) Yao, G.; Kang, L.; Li, J.; Long, Y.; Wei, H.; Ferreira, C. A.; Jeffery, J. J.; Lin, Y.; Cai, W. B.; Wang, X. D. Effective Weight Control via an Implanted Self-Powered Vagus Nerve Stimulation Device. *Nat. Commun.* **2018**, *9*, 5349.

(44) Li, Z.; Zhu, G. A.; Yang, R. S.; Wang, A. C.; Wang, Z. L. Muscle-Driven *In Vivo* Nanogenerator. *Adv. Mater.* **2010**, *22*, 2534–2537.

(45) Ouyang, H.; Liu, Z.; Li, N.; Shi, B. J.; Zou, Y.; Xie, F.; Ma, Y.; Li, Z.; Li, H.; Zheng, Q.; Qu, X. C.; Fan, Y. B.; Wang, Z. L.; Zhang, H.; Li, Z. Symbiotic Cardiac Pacemaker. *Nat. Commun.* **2019**, *10*, 1821.

(46) Zheng, Q.; Zhang, H.; Shi, B.; Xue, X.; Liu, Z.; Jin, Y.; Ma, Y.; Zou, Y.; Wang, X.; An, Z.; Tang, W.; Zhang, W.; Yang, F.; Liu, Y.; Lang, X.; Xu, Z.; Li, Z.; Wang, Z. L. *In Vivo* Self-Powered Wireless Cardiac Monitoring via Implantable Triboelectric Nanogenerator. *ACS Nano* **2016**, *10*, 6510–6518.

(47) Barolet, D. Light-Emitting Diodes (LEDs) in Dermatology. *Semin. Cutaneous Med. Surg.* **2008**, *27*, 227–338.